Metallurgist, Vol. 57, Nos. 11–12, March, 2014 (Russian Original Nos. 11–12, November–December, 2013)

A WELDABILITY STUDY OF AL–CU–LI 2198 ALLOY

V. Calogero,[1] G. Costanza,[2] S. Missori,[2]
A. Sili,[1] and M. E. Tata[2]

Al–Cu–Li alloys, conceived for automotive and aeronautic applications thanks to the high mechanical resistance/density ratio, exhibit weldability issues common to all light alloys. In this paper, the weldability of Al–Cu–Li 2198 alloy was studied by comparing features of welds carried out by two processes, the traditional arc welding and the friction stir welding (FSW). Welded joints were submitted to optical and SEM metallographic examinations with EDS microanalysis measurements. Mechanical characteristics were evaluated through microhardness tests and the instrumented indentation test FIMEC (Flat-top cylinder Indenter for MEchanical Characterization).

1. Introduction

The production of light alloys with a high mechanical resistance/specific density ratio meets the demands of automotive and aeronautic industries [1, 2, 3]. As is well known, Al alloys of the series 2000, containing Cu as the main alloy element, exhibit optimal mechanical properties after thermal treatment and are suitable for service temperature up to about 150°C [4, 5].

With the addition of elements like Mg and Li, it is possible to reduce the specific density and to improve the performance of Al alloys for structural applications [6, 7, 8], with the aim of increasing the utilization of composites materials. The Li element effectiveness is related to the fact that every 1 wt.% of Li in Al alloys decreases the density by about 3% and increases the Young modulus by about 6%. Weld solidification cracking is an issue common to many Al alloys [9, 10], depending on the relationship between solidification temperature range, alloy composition, and the nature of eutectic constituents formed during the last stages of solidification under thermal stresses due to the large solidification range and high thermal expansion coefficients [11]. Moreover, in the heat affected zone (HAZ), mechanical properties are reduced [12] and are related to the possible formation of macroscopic flaws (bead irregularity, cracks, porosity, etc.) and metallurgical defects in the weld metal.

Weld metal (WM) properties can be controlled through the utilization of filler materials having the appropriate composition and suitable for achieving satisfactory structures and composition after dilution with the base metal. In principle, the mechanical properties of the HAZ could be restored through an adequate post-weld heat treatment, but usually this is hardly feasible.

The evaluation of weldability is usually made by comparing mechanical properties of welded samples (hardness, yield point, tensile strength, toughness) with those of the base material [13]. Since Al–Cu–Li alloys are utilized in applications demanding high mechanical properties, welded joints are very important for the stability of welded components. Friction stir welding (FSW) represents an interesting joining technique for Al alloys as an alternative to conventional fusion welding processes [14]. The FSW technique need not reach the liquid state, and heat input is lower. Consequently, negative effects on mechanical properties in the HAZ are reduced [15, 16, 17].

In this paper, aiming to characterize the weldability of Al–Cu–Li 2198 alloy, welded samples using the electric arc process are compared with samples joined with FSW. Experimental work included optical and SEM metallographic examinations and EDS microanalysis. Mechanical properties were evaluated through Vickers microhardness tests and the instru-

[1] Department of Materials Engineering, University of Messina, Messina, Italy.
[2] Department of Mechanical Engineering, University of Rome "Tor Vergata," Rome, Italy.

 0026-0894/14/1112-1134

TABLE 1. Base Metal Nominal Composition – Al–Cu–Li 2198 Alloy (wt.%)

Si	Fe	Ni	Mn	Mg	Cr	Zn	Zr	Ti	Pb	Li	Cu	Al
0.03	0.04	0.01	0.01	0.32	0.01	0.02	0.11	0.03	0.01	1.0	3.3	balance

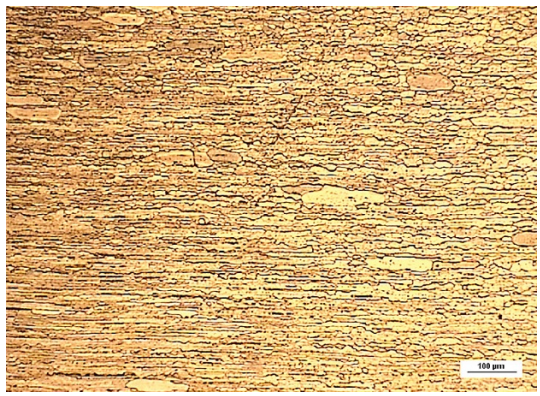

Fig. 1. Metallographic appearance of the Al–Cu–Li 2198 alloy plate as-supplied (condition T3).

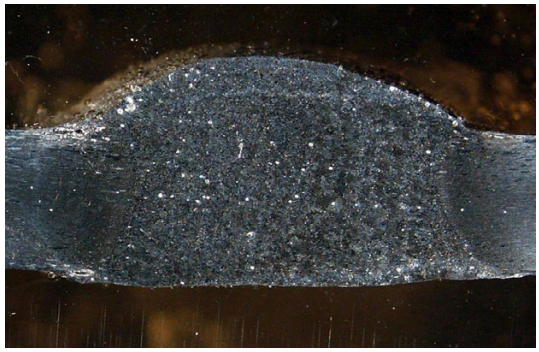

Fig. 2. Weld made with GTAW.

Fig. 3. Weld made with FSW.

mented indentation tests FIMEC (Flat-top cylinder Indenter for MEchanical Characterization), which are capable of estimating the local yield point in a small portion of material [18].

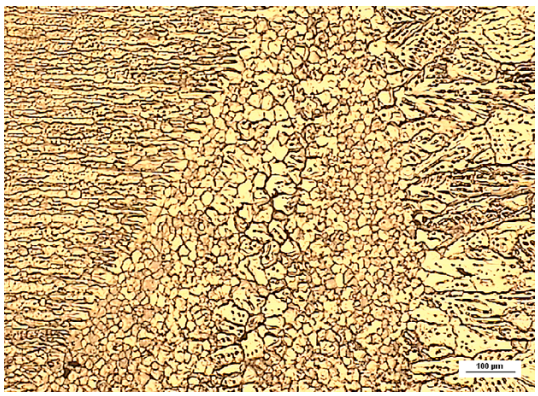

Fig. 7. Appearance of BM, HAZ, and FZ using optical micrographic examination.

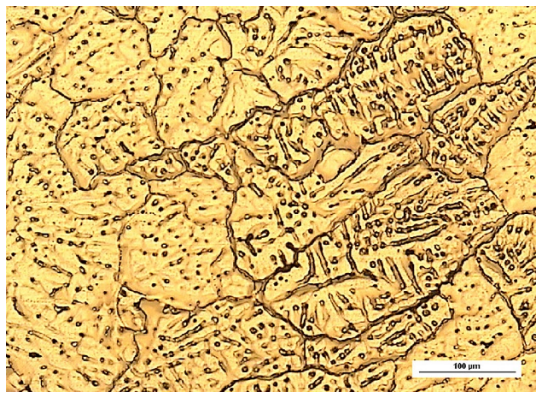

Fig. 8. Optical micrograph in the center of FZ.

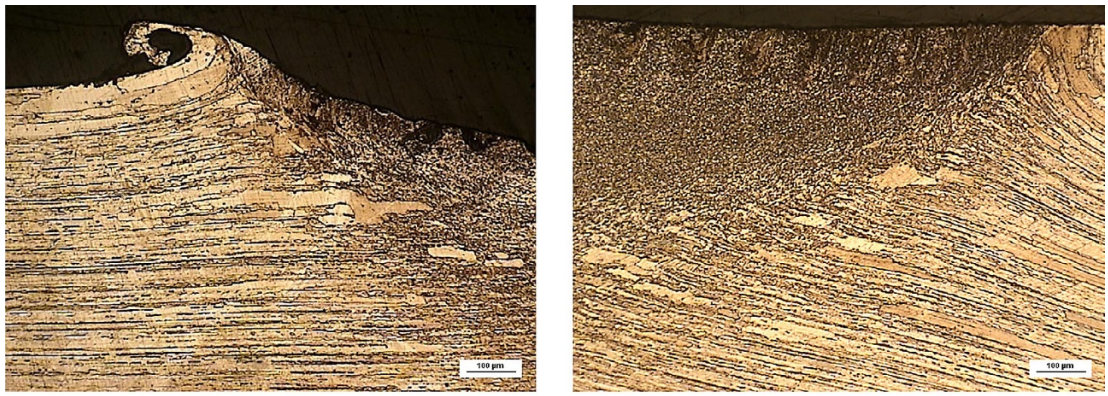

Sample A Sample B

Fig. 11. Optical micrographs of the cross section of the FSW joint.

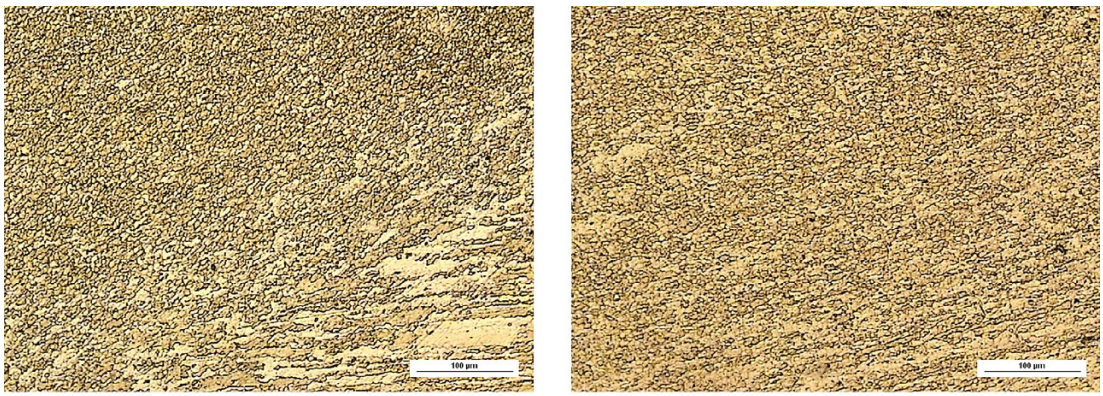

Sample A Sample B

Fig. 12. Optical micrographs of the cross section of the nugget in the region close to the boundary of TMAZ.

2. Materials and Methods

2.1. Al–Cu–Li 2198 alloy. The base metal (BM) is a plate of Al–Cu–Li 2198 alloy, 3 mm thick, submitted to a thermal treatment of solubilization, quench, plastic deformation, and natural aging (condition T3). The nominal composition is reported on Table 1.

The microscopic observation of base material microstructure shows grains elongated along the rolling direction with precipitates at the grain boundaries (Fig. 1).

2.2. Gas tungsten arc welding process. Plates of 2198 T3 alloy were butt welded by the gas tungsten arc welding process (GTAW), with square edges and no gap, after proper mechanical cleaning.

Abutting edges were held in proper alignment through tack welding.

The welding parameter for the GTAW process were:

Voltage . . . . . 12 V inverted polarity
Current . . . . . 98 A
Welding speed . . . . . 7 mm/sec
Inert gas (Ar) flow rate . . . . . 18 liters/min
Filler material. . . . . rods of alloy 2198

The filler material has the same composition as the base material. In such a way, the results can be easily compared with those achieved with the FSW process.

2.3. Friction stir welding process. Plates of 2198 T3 alloy were welded by FSW; a Cr–Mo steel tool, 12 mm diameter, with an end pin having a diameter 3/4 mm min/max and an angle of 2° from the vertical line, was utilized.

Welding was carried out with a rotation speed of 500 rpm and an advancing speed of 150 mm/min for sample A and 100 mm/min for sample B.

2.4. Metallographic samples. Samples for metallographic observations and microhardness tests were prepared by cutting the weldment normally to the welding direction. Samples were duly polished and etched with the Keller reagent (1.0 ml HF, 1.5 ml HCl, 2.5 ml HNO_3, 95 ml H_2O).

2.5. Microhardness Vickers and FIMEC tests. Microhardness Vickers tests were carried out on metallographic samples along a line transversally to the welding axis. The test load was 500 g applied for 15 sec. The indentation tests FIMEC with a cylindrical probe (diameter 1 mm) and advancing speed (0.1 mm/min) were carried out on the plate surface in several regions of the joints welded with both GTAW and FSW processes. During the FIMEC test, the values of the load were plotted as a function of the penetration depth. The values of the specific pressure are calculated as the load/probe area ratio.

3. Experimental Results and Discussion

3.1. Macrographic and micrographic observations. Samples welded with the two welding processes exhibit satisfactory metallographic appearance with full penetration and regular geometry with no visible macroscopic defects. Figures 2 and 3 show the macrographic appearance of welds carried out with the two processes, GTAW and FSW.

3.2. Microhardness Vickers tests

3.2.1. Joint welded by GTAW. Figure 2 reports Vickers microhardness measured on the weld cross section normal to the welding axis, with origin located on the same axis.

The values range around 110 HV in the base metal and reach a minimum in the region close to the welding axis. The width of the weld zone (WZ) showing the lowest hardness values is about 4 mm. No significant alteration of hardness consequent upon heating can be observed in the HAZ.

3.2.2. Joint welded by FSW. Microhardness values on samples carried out by FSW are not below the values on BM; hardness along a transversal cross section shows a fluctuating profile with some peaks in correspondence with the side limits of the nugget central zone and along the weld axis, as showed in Fig. 5, related to sample B.

3.3. FIMEC tests. The results of FIMEC tests are shown through pressure vs. penetration depth diagrams. These diagrams are characterized first through an elastic stage until a specific pressure p_L is reached, followed by a plastic deformation stage with an almost linear trend up to a pressure p_y, where a larger plastic deformation starts with a sharp variation of slope. Here a protrusion of material occurs around the indentation, followed by a constant slope deformation with a

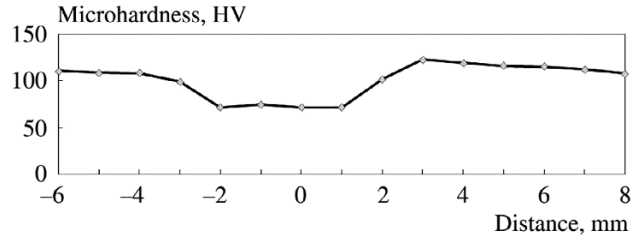

Fig. 4. Microhardness profile along a transverse line in the weld cross section with the GTAW process.

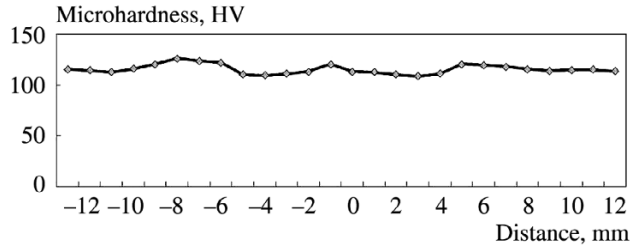

Fig. 5. HV microhardness profile along a transverse line in the cross section of sample B.

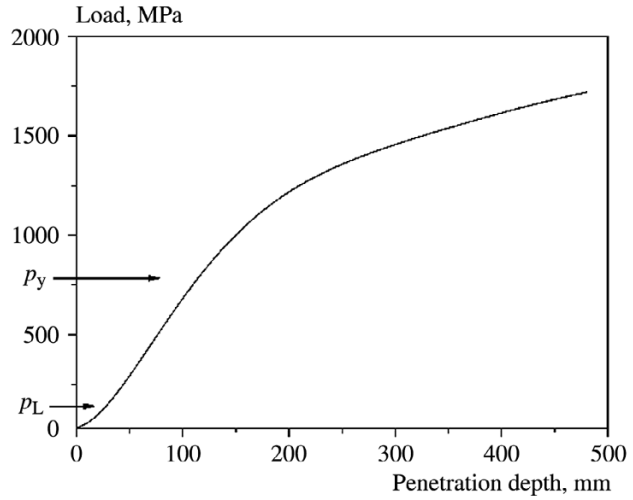

Fig. 6. FIMEC test: load vs. penetration depth diagram.

remarkable plastic flow. Figure 6 shows diagrams of the FIMEC tests on a sample of alloy 2198 (base metal): the arrows show the values p_L and p_y.

When the penetration speed is lower than 0.1 mm/min, the FIMEC test gives indications about the mechanical behavior of material submitted to the static tensile test with a speed of 10^{-3} sec^{-1}. Under these conditions, the following relationship, valid for several metal alloys [18], can be applied to estimate the yield strength (σ_y) and the load p_y evaluated through FIMEC test:

$$\sigma_y \approx p_y/3. \quad (1)$$

TABLE 2. Values of p_y and σ

	$p_y/3$, MPa; FIMEC test	σ_y, MPa; Tensile test [19]	Welding joint efficiency, %
Alloy 2198 T3	265	275	–
Joint FSW A	256	248	90
Joint FSW B	242	240	87
Joint GTAW	179	–	67

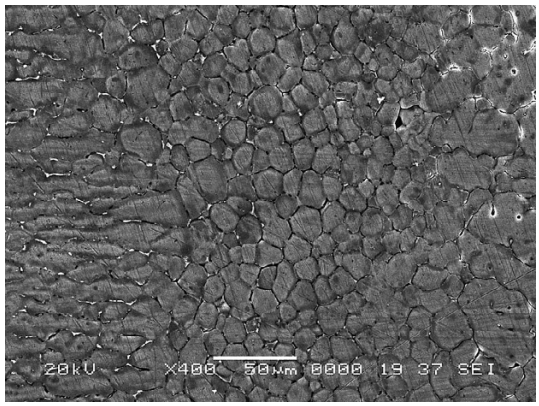

Fig. 9. Appearance of BM, HAZ, and FZ using SEM.

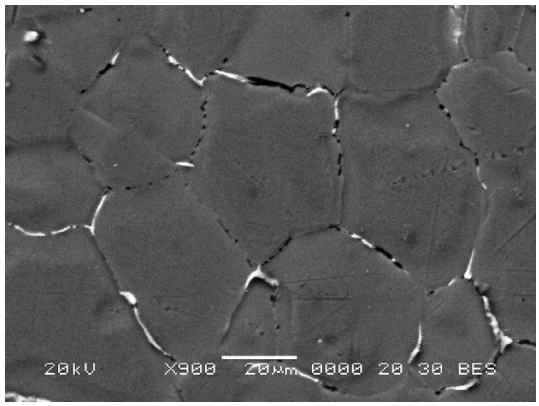

Fig. 10. SEM micrograph in FZ, outlining the precipitates at the grain boundaries.

The values of $p_y/3$ and σ_y for the base metal and welded joints are compared (see Table 2). The same Table also shows the welding efficiency of the welded joints, assumed to be the ratio between yield strength of welded joint and of the base metal. In the case of the GTAW joint, σ_y is estimated as equal to $p_y/3$ by the FIMEC test.

The values of $p_y/3$ fit quite well with the values σ_y. The efficiencies achieved with FSW are remarkably higher than with GTAW.

3.4. Micrographic observations and microanalysis measurements

3.4.1. Fusion welded joints. The transition from base metal to fusion zone microstructure has been observed through optical and SEM microscopy.

Optical microscopy observations. In Fig.7 from left to right are shown: a) the base metal with typical structure resulting from cold-rolling, b) a narrow heat affected zone, and c) the melt zone.

The HAZ has a width of 200–300 ∝m showing small equiaxial grains (about 20 ∝m), formed after a fast recrystallization. The fusion zone shows an epitaxial growth starting from unmelted grains. Farther from the fusion line, the structure consists of mainly dendritic crystals of larger size without a specific orientation (Fig. 8). Numerous precipitates of quite large size, mainly elongated, are visible along the grain boundaries and inside the grains.

The appearance of the same structures using SEM observations is shown in Figs. 9 and 10, with evidence of precipitate particles at grain boundaries.

As is well known, Al–Li–Cu alloys such as A2198 exhibit high strength levels due to the precipitation state achieved through a relatively complex precipitation sequence, which can involve solute clusters, GP zones, and θ′, T1, and δ′ phases [20, 21]. After welding, these structures undergo an evolution with the possible decrease of mechanical properties in the HAZ (i.e., due to the precipitation of the T1 phase at the grain boundaries). In our experiments, however, no appreciable reduction of mechanical strength nor of microhardness was revealed after laboratory tests. Our microanalysis measurements, made by EDS on a quite wide region in the FZ, allowed us to estimate the distribution of phases rich in Cu, which turned out to be much greater than in the BM. Unfortunately, this technique did not permit us to reveal the presence of particles containing Li and Mg.

3.4.2. FSW welded joints. In the central zone of the joint (nugget), the FSW process involves stirring of the material through the entire thickness, resulting in deep plastic deformation at elevated temperatures. The elongated grains of the parent metal are bent and broken to form, in the nugget, a structure made of recrystallized, very fine and equiaxial grains. Figure 11 shows a micrographic view of the stirred metal. The thermomechanically affected zone (TMAZ) is clearly visible with the typical nugget structure.

The joint A gave rise to a slightly better tensile resistance, as assessed both with tensile [19] and FIMEC tests. This could be ascribed to the finer structure of the nugget in sample A compared to the joint B (Fig. 12).

Conclusions

The quality of aluminum alloy welds can be affected by the possible formation of flaws and metallurgical transformations following the overheating processes, with reduction of mechanical properties. Generally the mechanical efficiency, which is an index of reduction of mechanical strength of the base metal, rarely exceeds 70%.

In our trials, joints welded with both traditional GTAW and innovative FSW processes showed good quality and soundness and were free from observable flaws. Joints carried out using GTAW, when submitted to microhardness survey and FIMEC tests, showed good mechanical properties. Welding efficiencies were equal to about 70%.

Joints carried out by FSW exhibited better mechanical properties and a greater welding efficiency, reaching a value of about 90%.

REFERENCES

1. R. T. Holt, A. K. Koul, L. Zhao, et al., “Lightweight materials for aircraft applications,” *Mater. Charact.*, **35**, No. 1, 41–67 (1995).
2. V. Wagner, “Evoluzione delle leghe di alluminio per aeronautica dopo le due guerre mondiali,” *Metall. Ital.*, No. 6, 9–21 (2005).
3. T. Warner, “Recently-developed aluminium solutions for aerospace applications,” *Mater. Sci. Forum*, **519/521**, 1271–1278 (2006).
4. K. S. Kumar, S. A. Brown, and J. R. Pickens, “Microstructural evolution during aging of an Al–Cu–Li–Ag–Mg–Zr alloy,” *Acta Mater.*, **44**, No. 5, 1899–1915 (1996).

5. S. P. Ringer and K. Hono, "Microstructural evolution and age hardening in aluminium alloys: atom probe field – ion microscopy and trasmission electron microscopy studies," *Mater. Charact.*, **44**, 101–131 (2000).
6. J. Ehrström and T. Warner, "Metallurgical design of alloys for aerospace structures," *Mater. Sci. Forum*, **331/337**, 5–16 (2000).
7. A. Heinz, A. Haszler, C. Keidel, et al., "Recent development in aluminium alloys for aerospace applications," *Mater. Sci. Eng. A*, **280**, No. 1, 102–107 (2000).
8. L. Bonaccorsi, G. Costanza, S. Missori, and M. E. Tata, "Mechanical and metallurgical characterization of 8090 Al–Li alloy welded joints," *Metallurgist*, **56**, No. 1–2, 75–84 (2012).
9. B. Irving, "Welding the four most popular aluminium alloys," *Weld. Int.*, **73**, No. 2, 51–55 (1994).
10. A. Kostrivas and J. C. Lippold, "Weldability of Li-bearing aluminium alloys," *Int. Mater. Rev.*, **44**, No. 6, 217–237 (1999).
11. G. D. Janaki Ram, T. K. Mitra, M. K. Raju, and S. Sundaresan, "Use of inoculants to refine weld solidification structure and improve weldability in type 2090 Al–Li alloy," *Mater. Eng.*, **A276**, 48–57 (2000).
12. G. O. Rading, M. Shamsuzzoha, and J. T. Berry, "A model for HAZ hardness profiles in Al–Li–X alloys: application to the Al–Li–Cu alloy 2095," *Weld. J.*, **77**, No. 9, 382s–387s (1998).
13. S. Missori and A. Sili, "Mechanical and microstructural properties of 8090 Al–Li alloy welded joints," *Metall. Sci. Technol.*, **20**, No. 2, 22–26 (2002).
14. P. Vilaca and W. Thomas, "Friction stir weldig technology," in: *Structural Connections for Lightweight Metallic Structures*, P. Moreira, L. da Silva, and P. de Castro (eds.), Advanced Structured Materials Ser., Springer-Verlag, Berlin, Heidelberg (2012), Vol. 8, pp. 85–124
15. P. Cavaliere, E. Cerri, and P. Leo, "Evoluzione meccanica e microstrutturale di una lega di alluminio 7075 saldata per friction stir welding," *Metall. Ital.*, No. 6, 33–39 (2005).
16. J. Adamowski and M. Szkodo, "Friction Stir Welding (FSW) of aluminium alloy AW6082-T6," *J. Achieve. Mater. Manuf. Eng.*, **20**, No. 1–2, 403–406 (2007).
17. K. Mroczka and A. Pietras, "FSW characterizations of 6082 aluminium alloys sheets," *Arch. Mater. Sci. Eng.*, **40**, No. 2, 104–109 (2009).
18. A. Donato, P. Gondi, R. Montanari, et al., "A remotely operated FIMEC apparatus for the mechanical characterization of neutron irradiated materials," *J. Nucl. Mater.*, **258–263**, 446–451 (1998).
19. C. Bitondo, U. Prisco, A. Squillace, et al., "Friction stir welding of AA2198-T3 butt joints for aeronautical applications," *Int. J. Mater. Form*, **3**, Suppl. 1, 1079–1082 (2010).
20. B. Decreus, A. Deschamps, and P. Donnadieu, "Understanding the mechanical properties of 2198 Al–Li–Cu alloy in relation with the intragranular and inter-granular precipitate microstructure," *J. Physics: Conf. Ser.*, **240**, 012096 (2010).
21. Li Cuia et al., "Effect of Nd:YAG laser welding on microstructure and hardness of an Al–Li based alloy," *Mater. Charact.*, **71**, 95–102 (2012).